Heliyon 10 (2024) e33051

Contents lists available at ScienceDirect

Heliyon

journal homepage: www.cell.com/heliyon

Research article

iTRAQ-based quantitative proteomics revealing the therapeutic mechanism of a medicinal and edible formula YH0618 in reducing doxorubicin-induced alopecia by targeting keratins and TGF-β/Smad3 pathway

Renkai Li [a,b,1], Mingxia Chen [a,1], Danxi Yan [a], Liang Chen [c], Mandi Lin [d], Bohui Deng [a], Likai Zhuang [a], Fei Gao [e], George Pak-Heng Leung [b,**], Jieshu You [a,*]

[a] College of Pharmacy, Shenzhen Technology University, Room 704, Block A2, 3002 Lantian Road, Pingshan District, Shenzhen, Guangdong Province, China
[b] Department of Pharmacology and Pharmacy, Li Ka Shing Faculty of Medicine, The University of Hong Kong, Hong Kong, China
[c] School of Exercise and Health, Shanghai University of Sport, Shanghai, China
[d] Department of Radiotherapy, The First Affiliated Hospital of Guangzhou University of Chinese Medicine, Guangzhou, Guangdong Province, China
[e] College of Pharmacy, Chengdu University of Traditional Chinese Medicine, Chengdu, Sichuan Province, China

ARTICLE INFO

Keywords:
Doxorubicin
Alopecia
Herbal formula
Proteomics
Network pharmacology

ABSTRACT

YH0618, a medicinal and edible formulation, has demonstrated the potential to alleviate doxorubicin-induced alopecia in animal studies and clinical trials. However, the mechanisms underlying its therapeutic effects remain unexplored. The objective of this study was to ascertain possible therapeutic targets of YH0618 in the treatment of doxorubicin-induced alopecia. The assessment of hair loss was conducted through the measurement of the proportion of the affected area and the examination of skin histology. Isobaric tags for relative and absolute quantification (iTRAQ) in quantitative proteomics was employed to discern proteins that exhibited variable expressions. The major proteins associated with doxorubicin-induced alopecia were identified using gene ontology (GO) and Kyoto Encyclopedia of Genes and Genomes (KEGG) pathway analysis. The interaction network of the differentially expressed proteins was constructed using the STRING database and the Python software. The study analyzed a total of 3894 proteins extracted from the skin tissue of mice. Doxorubicin treatment resulted in the upregulation of 18 distinct proteins, whereas one differential protein was found to be downregulated. The above effects were reinstated after the administration of the YH0618 therapy. The bioinformatic study revealed that the identified proteins exhibited enrichment in many biological processes, including

Abbreviations: BP, Biological Process; CIA, Chemotherapy-induced Alopecia; CC, Cellular Component; COG/KOG, Clusters of Orthologous Groups/euKaryotic Orthologous Groups; DOX, Doxorubicin; DTT, Dithiothreitol; DEPs, Differentially Expressed Proteins; FDA, Food and Drug Administration; GO, Gene Ontology; KEGG, Kyoto Encyclopedia of Genes and Genomes; Krt, Keratin; PPI, Protein-protein Interaction; SD, Standard Deviation; SDS, Sodium Dodecyl Sulfate; Smad3, Sma and MAD-related protein 3; STRING, Search Tool for the Retrieval of Interacting Genes/Proteins; TGF-β, Transforming Growth Factor-β; TCM, Traditional Chinese Medicine; TEAB, Tetraethylammonium Bromide; MF, Molecular Function.

* Corresponding author.
** Corresponding author.
E-mail addresses: gphleung@hku.hk (G.P.-H. Leung), youjieshu@sztu.edu.cn (J. You).
[1] These authors contributed equally to this work.

https://doi.org/10.1016/j.heliyon.2024.e33051
Received 26 March 2024; Received in revised form 7 June 2024; Accepted 13 June 2024
Available online 18 June 2024

staphylococcus aureus infection, estrogen signaling route, pyruvate metabolism, chemical carcinogenesis, and PPAR signaling pathway. The results of Western blot revealed that the levels of keratin 81 (Krt81), keratin 34 (Krt34), keratin 33a (Krt33a), and Sma and MAD-related protein 3 (Smad3) were upregulated in response to doxorubicin treatment, and were attenuated by the administration of YH0618. These four proteins are likely to correlate with DOX-induced alopecia and serve as promising therapeutic targets for YH0618. This work presents significant insights and empirical evidence for comprehending the process underlying chemotherapy-induced alopecia, paving the way for exploring innovative therapeutic or preventive strategies employing herbal items.

1. Introduction

Alopecia is a frequently observed adverse effect occurring in around 65 % of patients undergoing chemotherapy. The occurrence rate of alopecia induced by certain chemotherapy medications, such as doxorubicin and paclitaxel, can reach levels as high as 80%–100 % [1,2]. While alopecia may not pose a direct threat to individual life, it significantly diminishes the overall quality of life. This is primarily because of the continuous unpleasant emotions, including anxiety, despair, and negative self-evaluation, that are commonly reported by patients [3,4]. The precise molecular process underpinning the phenomenon of chemotherapy-induced alopecia (CIA) remains elusive and requires further investigation. The fundamental concepts for mitigating CIA involve minimizing the delivery of chemotherapeutic agents to the hair follicle and employing pharmaceutical interventions to facilitate hair regrowth [5]. Nevertheless, a viable solution to mitigate this issue has yet to be devised [2,4]. The sole method sanctioned by the United States is scalp cooling therapy. The Food and Drug Administration (FDA) has approved a treatment for CIA, but its efficacy rate is below 50 % [6]. In addition, individuals at a heightened risk of cold-induced urticaria, cold agglutinin illness, and cryoglobulinemia are not good candidates for scalp cooling therapy [7,8].

The utilization of Traditional Chinese Medicine (TCM) in treating cancer, either as a standalone therapy or as a complementary approach, has been well-documented [9,10]. The possible discordance between TCM and chemotherapy medications remains a significant area of concern for both medical practitioners and patients. Utilizing species with homology in medicine and food is widely perceived as a safer and more beneficial approach. In this context, a medicinal and edible formulation named YH0618 has been devised to mitigate the toxicity and adverse effects associated with chemotherapy. The composition of YH0618 includes Sojae Semen Nigrum (Hei Dou), Brown Rice (Cao Mi), Glycyrrhizae Radix et Rhizoma (Gan Cao), Auricularia polytricha (Mont.) Sacc (Hei Mu Er), and Siraitiae Fructus (Luo Han Guo), and its main active components were identified by UPLC analysis [11]. A recent randomized clinical research showed that the administration of YH0618 resulted in a considerable reduction in skin and nail pigmentation caused by chemotherapy. Additionally, it was demonstrated that YH0618 facilitated the regeneration and darkening of hair, ultimately improving the overall quality of life for individuals undergoing cancer treatment [12]. Furthermore, animal experiments demonstrated that YH0618 effectively reduced doxorubicin (DOX)-induced alopecia in C57BL/6 mice while not compromising the anticancer effects [12].

Despite the shown therapeutic efficacy of YH0618, there remains a dearth of research investigating its underlying mechanism of action. Proteomics assumes a pivotal position in drug discovery and development. This innovative approach enables the investigation of protein interactions, biological functionalities, and physical attributes. CIA is a complex process involving multiple factors and signaling pathways [13]. TCM exhibits a multifaceted mode of action by targeting various biological entities [14]. Network pharmacology is a valuable approach to constructing a network encompassing multiple components and targets, facilitating elucidation of the molecular mechanisms behind Chinese medicine formulations [15]. Therefore, the primary objective of this study is to employ proteomics and network pharmacology to thoroughly and comprehensively investigate the underlying mechanism by which YH0618 mitigates alopecia induced by DOX.

2. Materials and methods

2.1. Plant materials and preparation of YH0618

YH0618 consists of Sojae Semen Nigrum (Heidou), Brown Rice (Caomi), Glycyrrhizae Radix et Rhizoma (Gancao), Auricularia polytricha (Mont.) Sacc (Hei Muer) and Siraitiae Fructus (Luohanguo) at a ratio of 15:15:3:1:1 (w/w). Heidou, Caomi, and Hei Muer were purchased from Jilin Beixian Eco Agri-industries Group Co., Ltd. (Jilin, China). Luohanguo was purchased from Guilin Baishouyuan Food Co., Ltd. (Guangxi, China). Gancao was purchased from Shenzhen Heshun Materia Medica Co., Ltd. (Guangdong, China).

YH0618 was smashed into coarse particles and decocted with boiling distilled water three times (1:10, 1:8, and 1:8 w/v) for 1 h. The solution was filtered with gauze and concentrated by a rotary evaporator. The condensate was dehydrated by a freeze-dryer and stored at −80 °C.

2.2. Effect of YH0618 on DOX-induced alopecia

2.2.1. Animals

All animal experiments in this study were monitored and handled following an animal protocol (NO. 20200903002) approved by the Ethics Committee for Laboratory Animals, Guangzhou University of Chinese Medicine (Guangzhou, China). C57BL/6 mice (7 weeks old and weighed between 18 and 20 g) were supplied by the Laboratory Animal Center at Guangzhou University of Chinese Medicine. These mice were confirmed to be pathogen free. The mice were housed in a controlled environment with a temperature of 25 ± 2 °C, relative humidity ranging from 40 % to 60 %, and a light/dark cycle of 12 h each. The mice were accommodated for one week before the commencement of the studies, during which they were provided unrestricted access to food and water.

The experimental model was developed utilizing the previously proposed modified method [16]. The dorsal skin of the mice was treated with a depilatory cream, resulting in the removal of hair shafts within a designated region measuring 1.5 cm by 2 cm. The uniform pink hue of the skin indicated the presence of hairs in the telogen phase. Removing hair at this stage resulted in the simultaneous growth of new hair in the anagen stage. Based on the dose regimen outlined in Supplementary Tables S1 and 40 mice were allocated into four groups using random assignment. Each group consisted of 5 male and 5 female mice, and the groups were identified as the control group, YH0618 group, DOX group, and DOX + YH0618 group. The DOX and DOX + YH0618 groups were administered a 0.2 mL intraperitoneal injection of DOX (5 mg/kg) once weekly for 3 weeks. In contrast, the control and YH0618 groups were given an intraperitoneal injection of 0.2 mL vehicle alone. In addition, the YH0618 and DOX + YH0618 cohorts were subjected to intragastric injection of YH0618 at a dosage of 4.5 g/kg daily for 3 weeks. Conversely, the control and DOX groups were administered 0.9 % NaCl using the same method. Following a three-week treatment period, the mice were promptly euthanized under anesthesia. The skin samples were gathered to conduct subsequent analysis.

2.2.2. Hair loss evaluation

The skin color change and hair regrowth time in the depilated area were observed and recorded daily. The percentage of hair loss area (i.e., area without hair growth/area of the entire hair removal area × 100 %) was analyzed on the 0^{th}, 7th, 14th, and 21st day after hair removal.

2.2.3. Skin histopathology

The skin tissues were fixed with 4 % paraformaldehyde, embedded in paraffin, and sectioned. The tissue sections were stained with hematoxylin-eosin trichrome for histological evaluation under microscopy.

2.3. Exploration of mechanisms by proteomics

2.3.1. Protein sample preparation

Skin tissues were homogenized in sodium dodecyl sulfate (SDS) lysis buffer (1:5, w/v). The homogenates were centrifuged at 12,000×*g* for 10 min at 4 °C, and the supernatant was collected. The protein concentrations of each sample were quantified using the bicinchoninic acid protein assay kit (Thermo Fisher Scientific, MA, USA).

2.3.2. Protein digestion and iTRAQ labeling

The protein sample (50 μg) was used, and dithiothreitol (DTT) was added to the protein solution with the final concentration of 5 mM. The mixtures were incubated at 55 °C for 30 min and alkylated by adding iodoacetamide solution (final concentration of 5 mM) for 15 min at room temperature. Subsequently, acetone (1:6, w/v) was added for protein extraction overnight at −20 °C. The samples were centrifuged for 10 min (4 °C, 8000×*g*), and the precipitates were collected. The proteins were re-suspended in 100 mM tetraethylammonium bromide (TEAB) and digested with trypsin (in a ratio of protein: trypsin of 50:1) at 37 °C for 12 h. The mixtures were labeled using the iTRAQ Reagent-8 plex Multiplex Kit (Applied Biosystems, CA, USA) according to the manufacturer's protocol.

2.3.3. Fractionation by high pH reversed-phase (RP) chromatography

The iTRAQ-labeled peptide mixtures were fractionated by HPLC with a reverse phase column (Agilent Zorbax Extend-C18 column, 2.1 mm × 150 mm, 3 μm, Agilent Corporation, MA, USA). In the binary solvent system, mobile phase A was ACN-H_2O (2:98, v/v; pH 10.0, adjusted with ammonium hydroxide), and mobile phase B was ACN-H_2O (90:10, v/v; pH 10.0, adjusted with ammonium hydroxide). Separation was performed at a flow rate of 300 μL/min using a linear gradient: 0–8 min, 98 % A; 8–8.01 min, 98%–95 % A; 8.01–48 min, 95 %—75 % A; 48–60 min, 75-60 % A; 60–60.01 min, 60-10 % A; 60.01–70 min, 10 % A; 70—70.01 min, 10–98 % A; 70.01–75 min, 98 % A. Finally, 15 fractions were collected from 8 min to 60 min.

2.3.4. LC–MS/MS analysis

The peptide fractions were analyzed using a Q Exactive orbitrap mass spectrometer equipped with Easy-nLC 1200 (Thermo Fisher, MA, USA). The fractions were loaded into the precolumn at a flow rate of 350 nL/min and separated through the analytical column 75 μm × 150 mm (RP-C18, New Objective, USA). The mobile phase A contained 0.1 % formic acid (v/v) in water, whereas ACN was used as mobile phase B. The peptides were separated using a linear 90 min gradient: 0–1 min, 2–6% B; 1–52 min, 6–35 % B; 52–54 min, 35–90 % B; 54–60 min, 90 % B. Afterwards, the eluted peptides were analyzed by a mass spectrometer. The primary MS mass resolution was set at 120,000, the automatic gain control value was 3×10^6, and the maximum ion injection time was 30 ms. Full-scan MS spectra (*m/z* 350–1650) were acquired, and the 15 highest peaks were scanned by MS/MS. All MS/MS maps were acquired using

sequential high-energy collisional dissociation (HCD) with collision energy at 3. The resolution of MS/MS was 15,000, and the automatic gain control was 1×10^5. The maximum ion injection time was 54 ms, and the dynamic exclusion time was set at 40 s.

2.3.5. Bioinformatics analysis

Proteins were identified and analyzed with the Proteome Discover 2.4 (Thermo Fisher Scientific, MA, USA). Uniprot, Kyoto Encyclopedia of Genes and Genomes (KEGG), Gene Ontology (GO), and Clusters of Orthologous Groups/euKaryotic Orthologous Groups (COG/KOG) databases were adopted for obtaining annotation information and functions of the identified proteins. GO and KEGG pathway enrichment analyses of the identified differentially expressed proteins (DEPs) were performed using the clusterProfiler package in R. The Search Tool for the Retrieval of Interacting Genes/Proteins (STRING) was adopted to analyze the protein–protein interaction (PPI) network among the selected DEPs. Cytoscape 3.7.2 software was used to analyze the differential proteins and establish their interaction and Venn diagram.

2.4. Verification of target proteins by Western blot

Skin tissues of the mice in each group were homogenized in a lysis buffer containing protease inhibitors and phosphatase inhibitors. The lysates were centrifuged at 12,000×*g* for 10 min at 4 °C, and the supernatant was collected. The protein concentration was quantified by a bicinchoninic acid protein assay kit (Thermo Fisher Scientific, MA, USA). The protein samples were separated by SDS-PAGE and transferred onto a PVDF membrane (GE Healthcare, Freiburg, Germany). The membranes were blocked with 5 % (w/v) non-

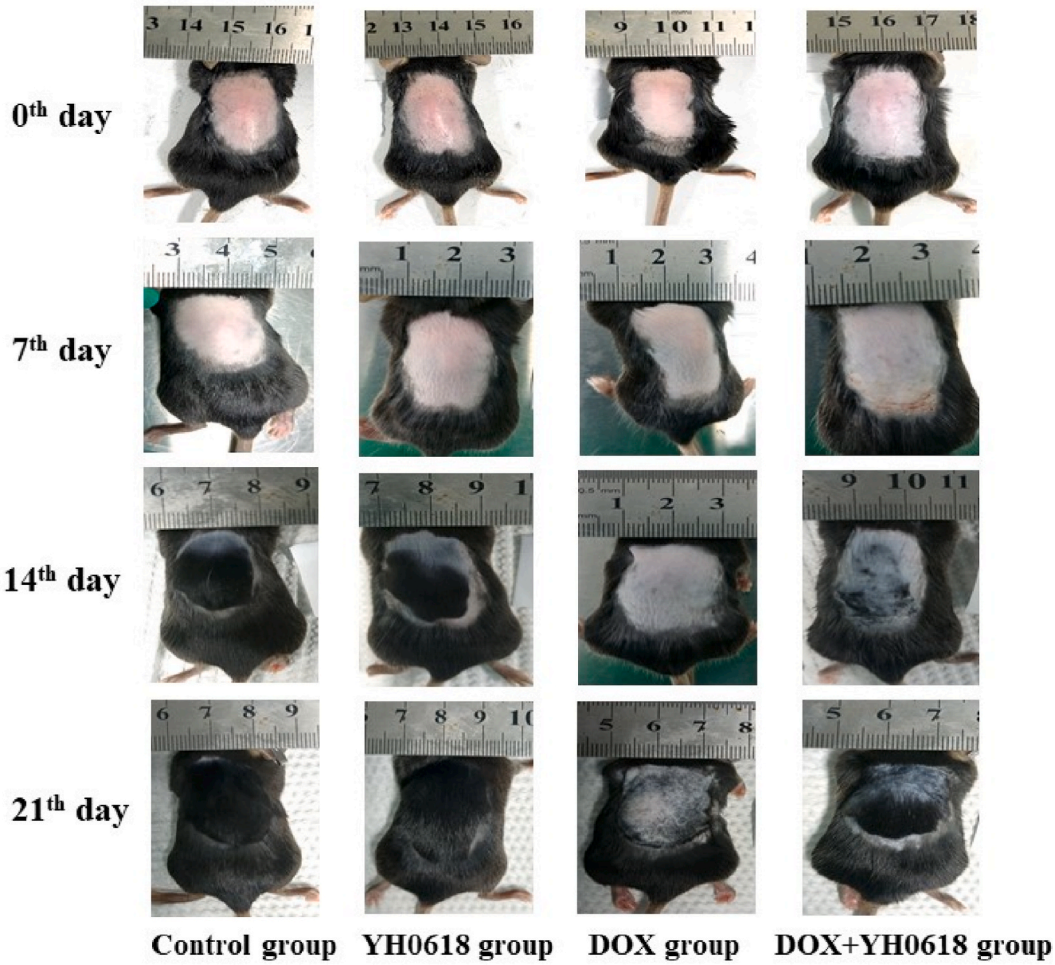

Fig. 1. Skin color changes and hair growth of mice at different time points of treatment. The hair shafts in an area of 1.5 cm × 2 cm were shaved. The dorsal skin of mice was treated with depilatory cream. The homogeneous pink color of the skin revealed the telogen phase of the hairs. Depilation at this hair stage induced the development of a synchronous anagen stage. The mice were randomly divided into the control group, YH0618 group, DOX group, and DOX + YH0618 group. After 3-week treatment, the mice were sacrificed under anesthesia. The skin samples were collected for further analysis. (For interpretation of the references to color in this figure legend, the reader is referred to the Web version of this article.)

fat milk powder in TBS with 0.1 % (v/v) Tween-20 for 1 h at room temperature, followed by incubation with primary antibodies, including keratin 81 (Krt81), keratin 34 (Krt34), keratin 33a (Krt33a), keratin 33b (Krt33b) and Sma and MAD-related protein 3 (Smad3) (Thermo Fisher Scientific, MA, USA) at 4 °C overnight. After washing with TBST, the membrane was incubated with corresponding secondary anti-mouse or anti-rabbit antibodies (Thermo Fisher Scientific, MA, USA) for 1 h at room temperature. The signals were visualized using the ECL Advance reagent (Seyotin, Guangzhou, China) and quantified using Tanon 4600 (Tanon, Shanghai, China).

2.5. Statistical analysis

The results were presented as the means ± standard deviation (SD) of at least 3 independent experiments. The data were analyzed by SPSS 25.0 software using normality tests, homogeneity of variance, and one-way analysis of variance (ANOVA) with LSD's or Bonferroni's multiple comparisons post hoc tests. The histogram for protein expression analysis was plotted using GraphPad Prism 8.0 software (GraphPad Software Inc., USA). $P < 0.05$ was considered statistically significant.

3. Results

3.1. Effect of YH0618 on DOX-induced alopecia

Fig. 1 and Table 1 present the physical characteristics of mouse skin and the quantification of hair loss area, respectively. On the 7th day of treatment, the dermal tissue of mice in both the control and YH0618 groups exhibited black pigmentation. In contrast, the dermal tissue of mice in the DOX group and the DOX + YH0618 group retained a pink coloration. No significant variation in the extent of hair loss area is observed among different groups. On the 14th day, the skin of all experimental groups exhibited a darkened pigmentation accompanied by hair growth. The control group and the YH0618 group had a considerably reduced proportion of hair loss area compared to the DOX group and the DOX + YH0618 group. Compared to the DOX group, the DOX + YH0618 group exhibited a slightly decreased percentage of hair loss area. However, this difference did not reach statistical significance. After 21 days of treatment, the control and YH0618 groups exhibited total hair regrowth in the shaved area. The DOX group showed a 33 % alopecia region. The co-administration of DOX with YH06118 resulted in a reduction of the proportion to 21 %.

3.2. Evaluation of YH0618 on skin histology

The study examined various pathological alterations in skin sections, including hyperemia, congestion, hemorrhage, edema, degeneration, necrosis, hyperplasia, fibrosis, organization, granulation tissue, and inflammatory changes. The findings indicated that the epidermis of mice in all experimental groups exhibited an intact structure with consistent thickness. The organization of the stratum corneum exhibited typical characteristics. The skin tissue showed no apparent signs of edema, congestion, or inflammatory response. On the 21st day, many hair follicles exhibiting consistent distribution and typical morphology were identified inside the dermis and adipose layer of mice in the control and YH0618 groups. Nevertheless, a few atrophic hair follicles were detected within the dermis and adipose tissue layer in the DOX group, with a notably sparse distribution. The DOX + YH0618 group had a larger quantity of hair follicles than the DOX group, and the distribution of hair follicles was uniform with typical morphology, as depicted in Fig. 2.

3.3. Proteomic analysis on the mechanisms of YH0618 on DOX-induced alopecia

3.3.1. Identification of DEPs

The iTRAQ analysis successfully identified 3894 proteins. 463 DEPs were identified in the DOX group compared to the control group, using the screening criteria of fold change (FC) greater than 1.2 or less than 0.83 and a significance threshold of p less than 0.05. Selecting upper and lower bounds for ratio thresholds is a common approach to identify differentially expressed proteins [17]. Although the threshold selections are variable, ratios greater than 1.2 or less than 0.83 were commonly regarded as differentially expressed [18]. Among these DEPs, 404 proteins exhibited an upregulated expression level, while 59 proteins showed a downregulated expression level. 102 DEPs were observed in the DOX + YH0618 group compared to the DOX group. Among these DEPs, 48 proteins were found to be up-regulated, while 54 proteins were down-regulated. The detected DEPs are included in Tables S2 and S3.

Table 1
Effect of YH0618 on DOX-induced hair loss area.

Group (n = 10)	0^{th} day Percentage of hair loss area (%)	7th day Percentage of hair loss area (%)	14th day Percentage of hair loss area (%)	21st day Percentage of hair loss area (%)
Control group	100	99.10 ± 1.73	13.70 ± 3.86[a]	4.10 ± 4.15[a]
YH0618 group	100	99.10 ± 1.37	14.30 ± 5.91[a]	6.60 ± 5.19[a]
DOX group	100	100	64.00 ± 17.13	33.20 ± 11.31
DOX + YH0618 group	100	100	58.50 ± 17.88	21.50 ± 10.39[a]

Compared with the DOX group.
[a] *Compared with DOX group , **P < 0.01*

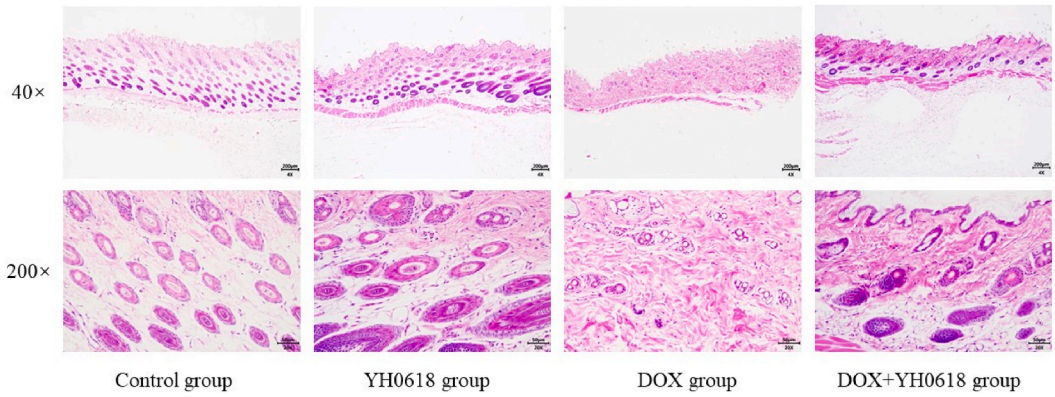

Fig. 2. Representative HE-stained sections of skin. The skin tissues were fixed with 4 % paraformaldehyde, embedded in paraffin, and sectioned. The tissue sections were stained with hematoxylin-eosin trichrome for histological evaluation under microscopy (40 × , 200 ×).

The volcanic maps were generated by considering two key factors: the fold change (Log2) between two distinct sample groups and the *p*-value (-Log10) derived from the *t*-test. These maps were employed to visually represent the notable changes observed between the control group and the DOX group, as well as between the DOX group and the DOX + YH0618 group (Fig. 3A and B). Additionally, the DEPs can be observed and analyzed from a macroscopic standpoint by generating a cluster heat map, as shown in Fig. 3C–D.

3.3.2. Cluster analysis of DEPs

To examine the specific protein targeted by YH0618 in the context of hair loss induced by DOX, a Venn diagram analysis was employed to conduct a more comprehensive assessment of the DEPs. The findings indicated a substantial increase in the expression levels of 386 proteins in the DOX group compared to the control group. Additionally, after treatment with YH0618, 18 of these proteins exhibited a significant decrease in expression (Fig. 4A). In contrast, the expression levels of 59 proteins exhibited a substantial decrease in the DOX group, whereas only one protein showed a significant increase following treatment with YH0618 (Fig. 4B). Table 2 displays a collection of 19 DEPs that have been reversed and are potentially the target proteins for YH0618 to mitigate DOX-induced alopecia.

3.3.3. GO analysis of reversed DEPs

The DEPs that were seen following the injection of YH0618 were utilized to conduct GO annotation and enrichment analysis, focusing on the domains of biological process (BP), molecular function (MF), and cellular component (CC). With respect to the examination of BP, the findings indicated that the DEPs influenced by YH0618 were primarily associated with the biosynthesis of acetyl CoA, the metabolic process of pyruvate, and the biosynthesis of lipids (Fig. 5). In the examination of CC, the identified DEPs were found to be linked with the cytosol, mitochondrion, and keratin filament. Upon analysis of MF, a significant proportion of the reversed DEPs exhibited relevance to structural molecular activity, calcium ion binding, and protein homodimerization activity.

3.3.4. KEGG pathway analysis of reversed DEPs

To determine the probable signaling pathway by which YH0618 reduces doxorubicin-induced alopecia, we conducted a KEGG signaling pathway analysis on the DEPs induced by YH0618 treatment. The signaling pathways implicated in the control of YH0618, as shown in Fig. 6, encompass staphylococcus aureus infection, estrogen signaling pathway, pyruvate metabolism, chemical carcinogenesis, and PPAR signaling system.

3.3.5. PPI analysis

To conduct a more comprehensive investigation into the reciprocal influence of the reversed DEPs resulting from YH0618 treatment, we utilized the STRING database and the Python tool "network" to evaluate these DEPs. The interaction network diagram displays 13 protein nodes and 25 interactions (Fig. 7). Notably, Krt81, Krt87, Krt34, Krt33b, Acly, Me1, Hrnr, Krt33a, and Gsta3 are positioned at the center of the network and serve as prominent hubs for interacting with other proteins.

3.4. Western blot analysis of the reversed DEPs

The DEPs that exhibit a close relationship with hair growth were chosen for further investigation using Western blot investigations. The findings indicate that the protein expression levels of Krt81, Krt34, Krt33a, and Smad3 were considerably elevated in the DOX group compared to the control group. Furthermore, the treatment with YH0618 resulted in a considerable reduction in the expression levels of these proteins. The protein expression level of Krt33b did not exhibit a statistically significant alteration in response to the treatment with DOX and YH0618, as demonstrated in Fig. 8A–B.

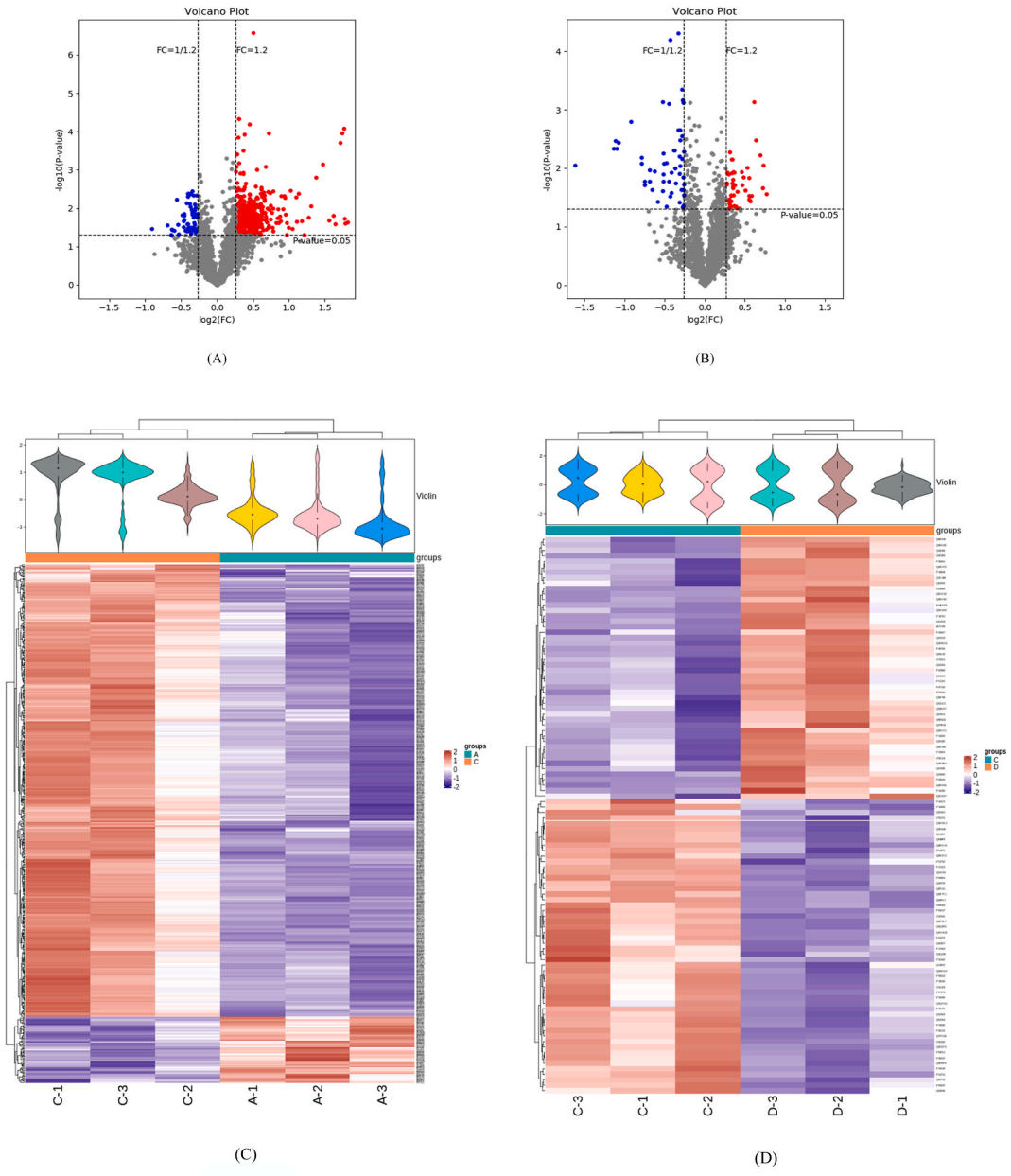

Fig. 3. iTRAQ quantitative proteomic analysis of DEPs after YH0618 treatment. Volcano plot was performed using the data of the proteins between the control group and DOX group (A), DOX group and DOX + YH0618 group (B) (Logarithmic transformation based on 10, Student's t-test). The significantly downregulated proteins were annotated in blue (FC < 0.83 and $P < 0.05$), the significantly upregulated proteins were annotated in red (FC > 1.2 and $P < 0.05$), and the proteins without differences were indicated in grey. Hierarchical clustering results between the control group and DOX group (C), DOX group and DOX + YH0618 group (D) were presented as a tree-type heatmap with the abscissa showing the samples and the ordinate showing the significant DEPs. The expression levels of the significantly differential proteins in different samples were exhibited in the heatmap by different colors after normalization using the log2 method, in which red dots represent the significantly upregulated proteins, blue dots represent the significantly downregulated proteins, and grey dots represent proteins with no quantitative information. (For interpretation of the references to color in this figure legend, the reader is referred to the Web version of this article.)

4. Discussion

The administration of DOX, a commonly used chemotherapeutic agent, has resulted in significant dermal-epidermal shrinkage and substantial modifications to the epithelial and mesenchymal constituents comprising hair follicles [19]. Prior research has indicated that the primary factor contributing to CIA is the apoptosis of matrix cells. This form of programmed cell death has been associated with various mechanisms, including alterations in p53 gene expression, decreased expression of β-catenin, glutathione depletion,

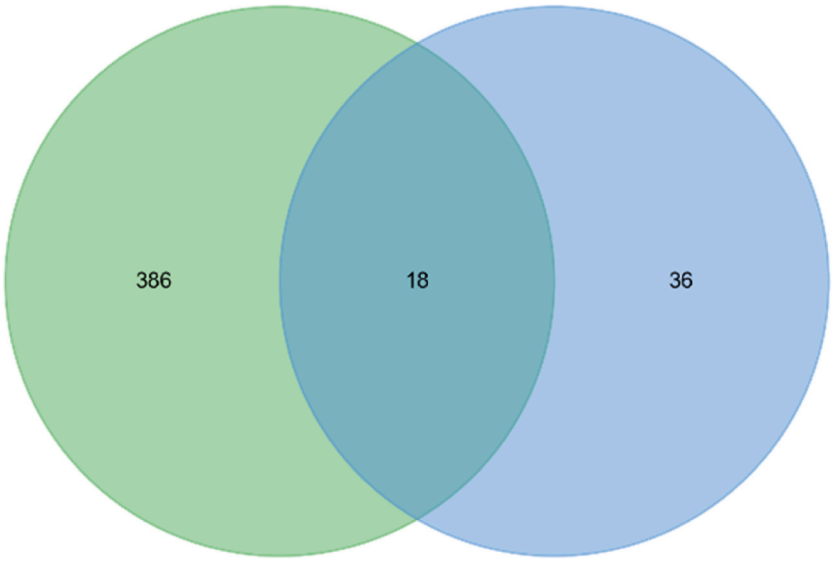

(A)

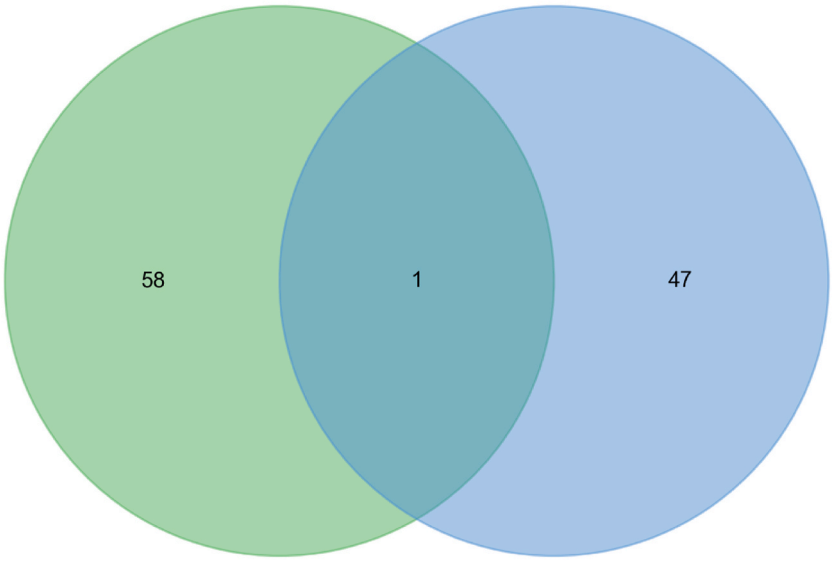

(B)

(caption on next page)

Fig. 4. A Venn diagram analysis of DEPs. (A) The green circle represents 386 up-regulated proteins in the DOX group compared with the control group; the blue circle represents 54 down-regulated proteins in the DOX + YH0618 group compared with the DOX group; the overlapping area presents 18 reversed differential proteins after YH0618 treatment. (B) The green circle represents 59 down-regulated proteins in the DOX group compared with the control group; the blue circle represents 48 up-regulated proteins in the DOX + YH0618 group compared with the DOX group; overlapping area presents 1 reversed differential protein after YH0618 administration. (For interpretation of the references to color in this figure legend, the reader is referred to the Web version of this article.)

Table 2
Reversed DEPs in mice skin tissue after YH0618 administration.

No.	Unitprot	Description	Gene Name	FC (D/C)	FC (Y + D/D)
1	Q91V92	ATP-citrate synthase	Acly	1.3624	0.7397
2	Q9Z2T6	Keratin, type II cuticular Hb5	Krt85	3.3930	0.5367
3	Q9ERE2	Keratin, type II cuticular Hb1	Krt81	3.3365	0.4628
4	Q6IMF0	Keratin, type II cuticular 87	Krt87	2.5990	0.4744
5	Q9D646	Keratin, type I cuticular Ha4	Krt34	3.2811	0.4552
6	Q8K0Y2	Keratin, type I cuticular Ha3-I	Krt33a	2.0331	0.6192
7	P06801	NADP-dependent malic enzyme	Me1	1.3551	0.6927
8	P17563	Methanethiol oxidase	Selenbp1	1.4172	0.6953
9	Q61897	Keratin, type I cuticular Ha3-II	Krt33b	2.7747	0.4656
10	P54731	FAS-associated factor 1	Faf1	1.4726	0.8073
11	Q8VHD8	Hornerin	Hrnr	1.7212	0.3256
12	Q9QXG4	Acetyl-coenzyme A synthetase, cytoplasmic	Acss2	1.2227	0.8283
13	Q8BVU5	ADP-ribose pyrophosphatase, mitochondrial	Nudt9	1.4181	0.8296
14	P11152	Lipoprotein lipase	Lpl	1.2313	0.7950
15	Q8BTY1	Kynurenine-oxoglutarate transaminase 1	Kyat1	1.6498	0.7341
16	P53702	Cytochrome c-type heme lyase	Hccs	1.2017	0.7774
17	P30115	Glutathione S-transferase A3	Gsta3	1.2632	0.7171
18	Q14BI2	Metabotropic glutamate receptor 2	Grm2	1.4392	0.7171
19	P14436	H-2 class II histocompatibility antigen, A-R alpha chain	H2-Aa	0.5334	1.3543

D/C: DOX group/Control group; Y + D/D: YH0618+DOX group/DOX group.

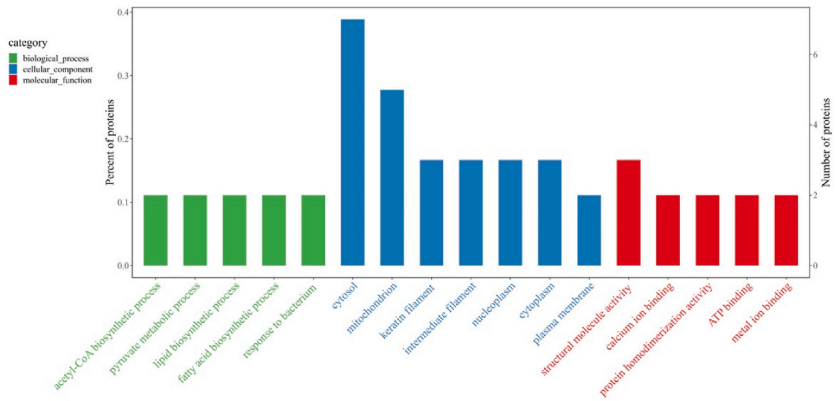

Fig. 5. GO analysis of the reversed DEPs in mice skin tissue after YH0618 administration. The abscissa represents the GO entry name, and the ordinate represents the number and percentage of proteins corresponding to the entry.

changes in mitochondrial function, and the production of reactive oxygen species [20,21]. The concept of oncosis has been suggested as an additional etiological factor contributing to CIA. The impact of DOX on glucose transport during the initial phase may decrease glycogen levels within the outer root sheath cells of hair follicles, ultimately culminating in oncosis [22]. Furthermore, suppressing angiogenesis and sebaceous gland dysfunction induced by DOX may contribute to hair loss [23,24]. The etiology of hair loss caused by DOX is multifaceted. Utilizing omics technology presents a significant methodological approach for systematically examining the mechanism underlying DOX-induced alopecia. Furthermore, it enables the exploration of the mechanisms through which potential protective medicines can mitigate this issue. The utilization of proteomics and network pharmacology has been employed to elucidate the underlying mechanism of action of TCM [25–27]. Previous works reported that C57BL/6 mice were set as the animal model to study alopecia. This model can well reflect the hair grown which possesses some advantages, such as recognition of mature hair follicles by pigmentation, maintaining a level of consistency, and testing the anagen-phased follicle that produces hair growth [28,29]. The present work used several methodologies to investigate the underlying mechanism by which the medicinal and edible formula YH0618 mitigates hair loss induced by DOX in C57BL/6 mice.

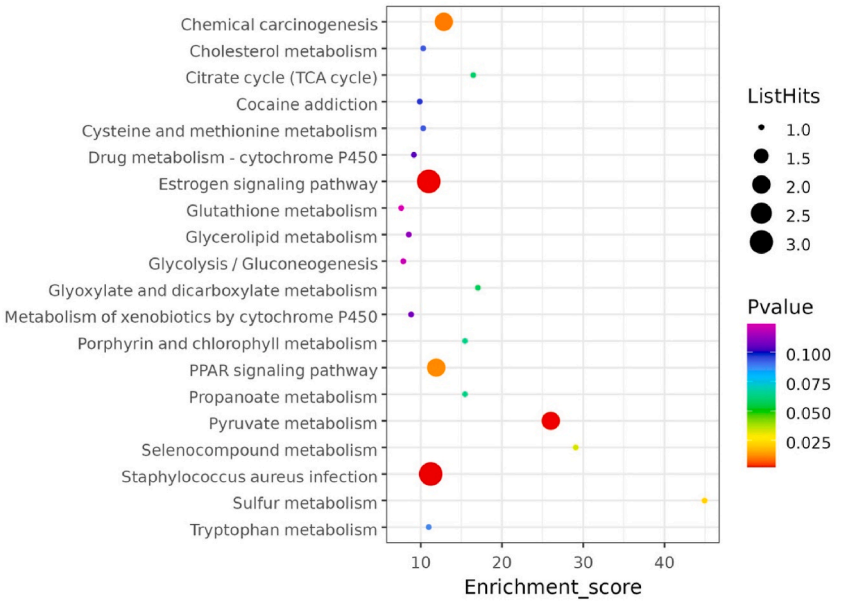

Fig. 6. KEGG pathway analysis of the reversed DEPs in mice skin tissue after YH0618 treatment. The abscissa represents the enrichment score, and the ordinate represents the pathway information with the top 20 enrichment score. The color changing from red and green to blue and violet represents the *p*-value. The bubble size represents the number of significant modular proteins, with a larger area indicating a greater number of proteins. (For interpretation of the references to color in this figure legend, the reader is referred to the Web version of this article.)

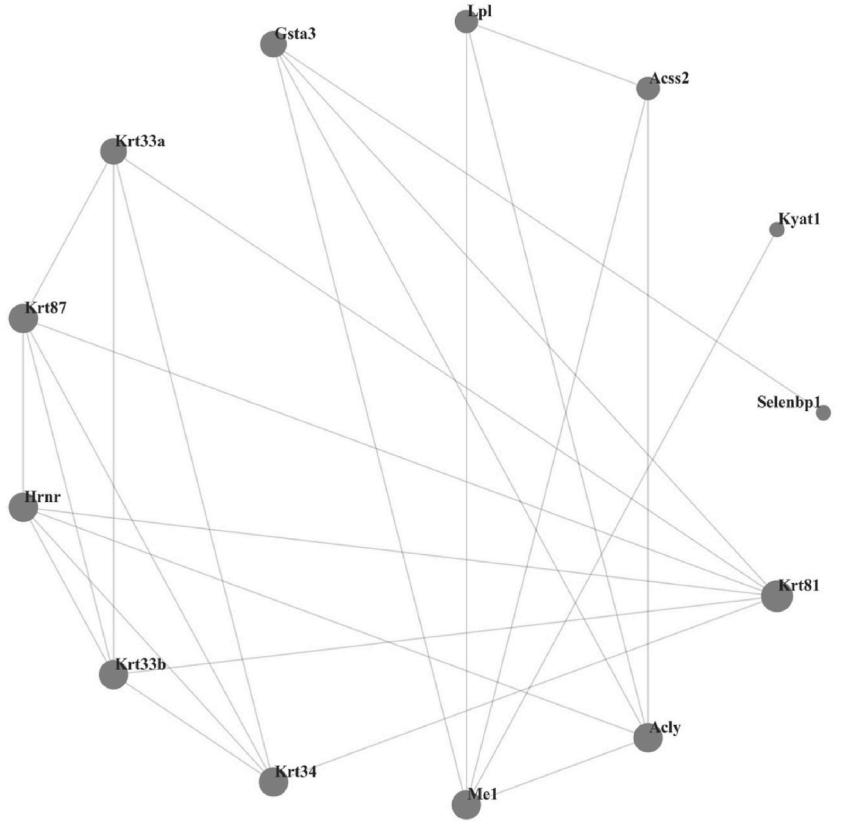

Fig. 7. PPI analysis of DEPs affected by YH0618 treatment. Circles represent differential proteins/genes. The size of circles represents the degree of connectivity, with larger circles indicating higher connectivity.

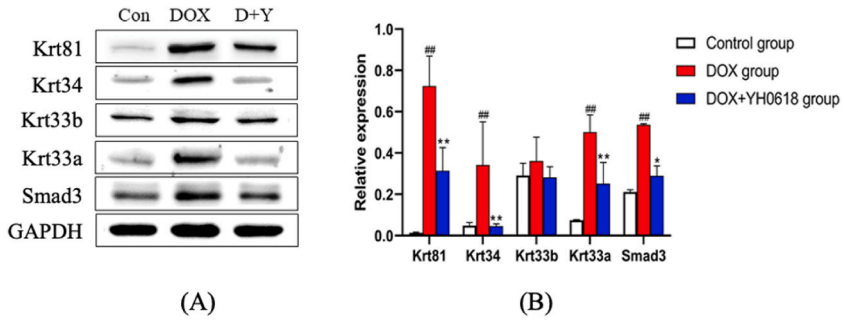

Fig. 8. Western blot analysis of Krt81, Krt34, Krt33a, Krt33b, and Smad3. Skin tissues of the mice were collected for Western blotting analysis. (A) The expressions of Krt81, Krt34, Krt33a, Krt33b, and Smad3 were analyzed by Western blotting. (B) Quantitative analysis of related protein bands and the intensities of them were normalized to that of GAPDH bands. The original blots were included in Supplementary Material (Fig. S1). $^{\#}$represents a significant difference compared to the control group ($^{\#}P < 0.05$; $^{\#\#}P < 0.01$); *represents significant difference compared to the DOX group ($^{*}P < 0.05$; $^{**}P < 0.01$).

The current investigation employed the iTRAQ-based quantitative proteomics technique to identify a total of 3894 proteins from the skin tissue of mice. Nineteen DEPs were shown to be impacted by DOX treatment. However, it was observed that these DEPs might be alleviated by applying the YH0618 treatment. The bioinformatics research revealed that the DEPs were implicated in several biological processes, including staphylococcus aureus infection, estrogen signaling pathway, pyruvate metabolism, chemical carcinogenesis, and PPAR signaling system. *Staphylococcus aureus* infection has been proven to be closely related to folliculitis, which can cause damage and necrosis of the hair follicle roots, leading to hair loss [30,31]. Some studies also found that estrogen receptors are expressed in the scalp hair follicles, and estrogen regulates the growth cycle and function of hair follicles through binding to estrogen receptors [32]. When the estrogen receptor pathway is abnormal, it may affect the normal physiological process of hair follicles, resulting in the occurrence or aggravation of hair loss [33]. Flores et al. showed that regulation of pyruvate entry into mitochondria for subsequent oxidation to fuel the TCA cycle can manipulate hair follicle stem cells and the hair cycle in normal adult mice with typical hair cycling, and also propose inhibition of pyruvate entry into mitochondria as a versatile treatment strategy for alopecia in humans [34]. PPAR is essentially a class of ligand-dependent transcriptional regulators, including three subtypes: PPARα, PPAR β/δ, and PPARγ [35]. Due to the breadth and complexity of the PPAR signaling pathway, it is known to be associated with many proteins, factors, and diseases. Hu et al. have developed a PPARγ agonist that can treat hair loss, which can upregulate the expression of iNOS genes, thereby promoting hair growth [36]. Therefore, the potential mechanism by which YH0618 reduces doxorubicin-induced alopecia appears to entail modulation of energy metabolism, hormone control, and inflammatory response.

Keratin serves as the primary structural constituent of epithelial tissues and hair and nails. The cellular structure is maintained, and various biological processes, including cell proliferation, migration, and apoptosis, are regulated by it [37,38]. Over the past three decades, several hair follicle-specific epithelial keratins, specifically those found in the root sheath and hair keratins, have been identified. The expression of type I keratin (Krt25-Krt28) and type II keratin (Krt71-Krt75) is localized primarily to the root sheath of hair follicles. On the other hand, hair keratins contain Type I keratin (Krt31, Krt32, Krt33a, Krt33b, Krt34-Krt40) and Type II keratin (Krt81-Krt86), as reported in a previous study [39]. Specific keratins are linked to hair abnormalities [40]. As an illustration, it has been observed that mutations occurring in the hard keratins Krt81 can result in monilethrix, which is classified as an autosomal dominant hair condition [41]. Besides, Giesen et al. [42] postulated that the observed drop in the expression levels of Krt33a and Krt34, two markers associated with the later stage of hair follicle differentiation, may contribute to the alterations in hair structure commonly observed during aging. The protein Krt33b, which exhibits an encoded structure, is associated with the development of hair and nails [43–45]. In the present study, the proteomic data revealed the involvement of four DEPs (Krt81, Krt34, Krt33a, and Krt33b) in the underlying mechanism of YH0618's activity in mitigating DOX-induced alopecia. The confirmation of the involvement of Krt81, Krt34, and Krt33a can be achieved using Western blot analysis. The findings of our investigation diverged from previous research, which indicated that the expressions of Krt33a, Krt33b, Krt34, and Krt81 were down-regulated in injured skin [46,47]. In contrast, our work demonstrated that DOX up-regulated the expressions of these proteins in the skin. The observed phenomenon may be attributed to the activation of alternative signaling pathways by DOX, resulting in alterations in the expression of these proteins. Further investigation is warranted to elucidate the precise underlying mechanism.

The transforming growth factor-β (TGF-β) protein plays a vital role in various biological processes, including embryonic development, organ formation, physiological remodeling of connective tissue during tissue repair and wound healing, and the development of cancer [48]. The Smads protein family is known to have a significant role in facilitating the transportation of TGF-β signal from the cell surface receptor to the nucleus [49]. Furthermore, distinct Smads mediate diverse signal transduction pathways of members of the TGF-β family. Prior research has established that the administration of high-dose electric radiation can lead to the development of skin thickening, fibrosis, permanent alopecia, and ulceration. Radiation exposure has been found to induce a significant upregulation of Smad3 protein expression in skin tissue, decreasing skin elasticity and bursting strength [50]. Furthermore, previous studies have indicated a correlation between hair development and hair follicle regeneration with the TGF-β/Smad3 signaling cascades [51,52]. In the present investigation, the administration of DOX resulted in an upregulation of Smad3 protein expression, a finding that aligns with previous studies [53,54]. Notably, the observed effect was mitigated by the application of YH0618. There is a possibility that the

TGF-β/Smad3 signaling pathway could be linked to alopecia generated by DOX, suggesting that it may serve as a viable therapeutic target for YH0618. Additional investigation is necessary to validate this theory.

Although we found that Krt33a, Krt33b, Krt34, Krt81, and TGF-β/Smad3 signaling pathway might be associated with the action of YH0618 in reducing DOX-induced alopecia, alopecia is a complicated progress after chemotherapy. There are two major types of CIA, including telogen effluvium and anagen effluvium [55], which may make the physiological process of CIA more complex and unpredictable. Previous research demonstrated that topical treatment of cyclin-dependent kinase-2 (CDK-2) decreased CIA at the application site in some tested rats [56]. In animal models, treatments of fibroblast growth factor and epidermal growth factor have demonstrated a preventative function for CIA [57,58]. It has been revealed that p53-deficient mice do not develop CIA, probably as a result of suppression of hair follicle apoptosis [59]. Further study is necessary to validate the relationships between the actions of YH0618 and the potential targets reported above. So far, the present investigation just focuses on the potential mechanism of actions of YH0618 on animal models and has not been extended to study the underlying relationship between hair regrowth and alopecia in patients after treatment. Further investigations are warranted to confirm whether the actions of YH0618 were related to the potential targets mentioned above in preventing CIA under the clinical application.

5. Conclusion

In summary, our research has provided evidence that the medicinal and edible formula YH0618 can mitigate hair loss induced by DOX and facilitate hair regrowth. The underlying mechanism is likely associated with signaling pathways related to energy metabolism, hormone control, and inflammatory response. Possible targets of YH0618 include Krt81, Krt34, Krt33a, and the TGF-β/Smad3 signaling pathway. This study aims to contribute novel insights and empirical evidence towards elucidating the underlying mechanism of CIA. Additionally, it sheds light on discovering possible therapeutic targets for preventing and treating CIA. The outcomes of this research endeavor will establish a solid groundwork for the subsequent investigation and development of pharmaceutical and nutraceutical interventions.

Availability of data and materials

The data used to support the findings of this study are available from the corresponding author upon request.

Ethics approval and consent to participate

All animal experiments in this study were monitored and handled following an animal protocol (NO. 20200903002) approved by the Ethics Committee for Laboratory Animals, Guangzhou University of Chinese Medicine (Guangzhou, China).

Consent for publication

All authors consent to the publication of this work in Heliyon.

Funding

The study was supported by the Natural Science Foundation of Top Talent of SZTU (grant no. GDRC202123) and by the National Natural Science Foundation of China (grant no. 81904272).

CRediT authorship contribution statement

Renkai Li: Writing – review & editing, Writing – original draft, Validation, Software, Methodology, Investigation, Formal analysis, Data curation. **Mingxia Chen:** Writing – review & editing, Writing – original draft, Investigation, Formal analysis, Data curation. **Danxi Yan:** Writing – original draft, Validation, Software, Methodology. **Liang Chen:** Writing – review & editing, Writing – original draft, Methodology, Investigation. **Mandi Lin:** Writing – original draft, Software, Resources, Methodology, Conceptualization. **Bohui Deng:** Writing – original draft, Software. **Likai Zhuang:** Writing – review & editing, Writing – original draft, Software. **Fei Gao:** Writing – review & editing, Writing – original draft, Resources, Conceptualization. **George Pak-Heng Leung:** Writing – review & editing, Writing – original draft, Supervision, Resources, Conceptualization. **Jieshu You:** Writing – review & editing, Writing – original draft, Supervision, Project administration, Funding acquisition, Conceptualization.

Declaration of competing interest

The authors declare that they have no known competing financial interests or personal relationships that could have appeared to influence the work reported in this paper.

Acknowledgements

We express our most sincere gratitude to all the professionals who selflessly participated in this study.

Appendix A. Supplementary data

Supplementary data to this article can be found online at https://doi.org/10.1016/j.heliyon.2024.e33051.

References

[1] H. West, Chemotherapy-induced hair loss (alopecia), JAMA Oncol. 3 (8) (2017) 1147, https://doi.org/10.1001/jamaoncol.2017.1026.
[2] R. Paus, I. Haslam, A.A. Sharov, V.A. Botchkarev, Pathobiology of chemotherapy-induced hair loss, Lancet Oncol. 14 (2) (2013) E50–E59, https://doi.org/10.1016/S1470-2045(12)70553-3.
[3] V. Boland, A.M. Brady, A. Drury, More than the loss of hair: the experience of chemotherapy-induced alopecia for women: an integrative review, Ann. Oncol. 32 (2021) S1279–S1280, https://doi.org/10.1016/j.annonc.2021.08.697.
[4] B. Rubio-Gonzalez, M. Juhasz, J. Fortman, N.A. Mesinkovska, Pathogenesis and treatment options for chemotherapy-induced alopecia: a systematic review, Int. J. Dermatol. 57 (12) (2018) 1417–1424, https://doi.org/10.1111/ijd.13906.
[5] M. Sikora, L. Rudnicka, Chemotherapy-induced alopecia - the urgent need for treatment options, J. Eur. Acad. Dermatol. 33 (2) (2019) E69–E70, https://doi.org/10.1111/jdv.15207.
[6] C.J. Dunnill, W. Al-Tameemi, A. Collett, I.S. Haslam, N.T. Georgopoulos, A clinical and biological Guide for Understanding chemotherapy-induced alopecia and its prevention, Oncol. 23 (1) (2018) 84–96, https://doi.org/10.1634/theoncologist.2017-0263.
[7] E.G. Grevelman, W.P.M. Breed, Prevention of chemotherapy-induced hair loss by scalp cooling, Ann. Oncol. 6 (3) (2015) 352–358, https://doi.org/10.1093/annonc/mdi088.
[8] S.A. Forsberg, Scalp, cooling therapy and cytotoxic treatment, Lancet 357 (9262) (2001) 1134, https://doi.org/10.1016/S0140-6736(00)04293-8.
[9] S. Chen, A. Flower, A. Ritchie, J.P. Liu, A. Molassiotis, H. Yu, et al., Oral Chinese herbal medicine (CHM) as an adjuvant treatment during chemotherapy for non-small cell lung cancer: a systematic review, Lung, Cancer 68 (2) (2010) 137–145, https://doi.org/10.1016/j.lungcan.2009.11.008.
[10] X.L. Liu, M.G. Li, X.H. Wang, Z.B. Dang, L.H. Yu, X.B. Wang, et al., Effects of adjuvant traditional Chinese medicine therapy on long-term survival in patients with hepatocellula carcinoma, Phytomedicine 62 (2019), https://doi.org/10.1016/j.phymed.2019.152930.
[11] J. You, Y. He, H. Zhi, V.H. Lee, S. Chan, L. Lao, et al., Effect of a medicinal and edible decoction YH0618 on chemotherapy-induced dermatologic toxicity: a randomized controlled trial, Ann. Transl. Med. 9 (1) (2021) 4, https://doi.org/10.21037/atm-20-5181.
[12] J.S. You, F. Gao, H.L. ang, F. Peng, L. Jia, K. Huang, et al., A medicinal and edible formula YH0618 ameliorates the toxicity induced by Doxorubicin via regulating the expression of Bax/Bcl-2 and FOXO4, J. Cancer 10 (16) (2019) 3665–3677. https://www.jcancer.org/v10p3665.htm.
[13] L. Wang, W.R. Xu, L. Cao, T. Tian, M.F. Yang, Z.M. Li, et al., Differential expression of proteins associated with the hair follicle cycle - proteomics and bioinformatics analyses, PLoS One 11 (1) (2016), https://doi.org/10.1371/journal.pone.0146791.
[14] Y.X. Jiang, Y. Chen, Y. Yang, X.X. Chen, D.D. Zhang, Screening five Qi-Tonifying herbs on M2 phenotype macrophages, Evid-Based. Compl. Alt. 2019 (2019), https://doi.org/10.1155/2019/9549315.
[15] Z.C. Zhou, B. Chen, S.M. Chen, M.Q. Lin, Y. Chen, S. Jin, et al., Applications of network pharmacology in traditional Chinese medicine research, Evid-Based. Compl. Alt. 2020 (2020), https://doi.org/10.1155/2020/1646905.
[16] R. Paus, B. Handjiski, S. Eichmuller, B.M. Czarnetzki, Chemotherapy-induced alopecia in mice. Induction by cyclophosphamide, inhibition by cyclosporine A, and modulation by dexamethasone, Aust. J. Pharm. 144 (4) (1994) 719–734. PMCID: PMC1887229.
[17] G.H. Elizabeth, H.S. John, C.W. Susana, H.S. Elizabeth, L.O. Ann, E.P. Jeanette, M. Terry, L. Kevin JPR. 7 (8) (2008) 3091–3101, https://doi.org/10.1021/pr070520u.
[18] S. Kamran, K. Laura, S.M. Marjorie, G.B. James, M. Ignacio, et al., Stem Cell. Dev. 15 (3) (2006) 461–470, https://doi.org/10.1089/scd.2006.15.461.
[19] S. Selleri, F. Arnaboldi, L. Vizzotto, A. Balsari, C. Rumio, Epithelium-mesenchyme compartment interaction and oncosis on chemotherapy-induced hair damage, Lab. Invest. 84 (11) (2004) 1404–1417, https://doi.org/10.1038/labinvest.3700170.
[20] K. Jahnukainen, T. Jahnukainen, T.T. Salmi, K. Svechnikov, S. Eksborg, O. Soder, Amifostine protects against early but not late toxic effects of doxorubicin in infant rats, Cancer Res. 61 (17) (2001) 6423–6427. https://aacrjournals.org/cancerres/article/61/17/6423/507825.
[21] R. Cece, S. Cazzaniga, D. Morelli, L. Sfondrini, M. Bignotto, S. Menard, et al., Apoptosis of hair follicle cells during doxorubicin-induced alopecia in rats, Lab. Invest. 75 (4) (1996) 601–609. PMID: 8874390.
[22] A. Mailloux, K. Grenet, A. Bruneel, B. Beneteau-Burnat, M. Vaubourdolle, B. Baudin, Anticancer drugs induce necrosis of human endothelial cells involving both oncosis and apoptosis, Eur. J. Cell Biol. 80 (6) (2001) 442–449, https://doi.org/10.1078/0171-9335-00171.
[23] S. Selleri, H. Seltmann, S. Gariboldi, Y.F. Shirai, A. Balsari, C.C. Zouboulis, et al., Doxorubicin-induced alopecia is associated with sebaceous gland degeneration, J. Inv. Der. 126 (4) (2006) 711–720, https://doi.org/10.1038/sj.jid.5700175.
[24] Y. Amoh, L.N. Li, M. Yang, P. Jiang, A.R. Moossa, K. Katsuoka, et al., Hair follicle-derived blood vessels vascularize tumors in skin and are inhibited by doxorubicin, Cancer Res. 65 (6) (2005) 2337–2343, https://doi.org/10.1158/0008-5472.CAN-04-3857.
[25] X. Lv, H.J. Wang, R.M. Wu, X.Y. Shen, G. Ye, The active compounds of yixin ningshen tablet and their potential action mechanism in treating coronary heart disease- A network pharmacology and proteomics approach, Evid-Based Compl. Alt. 2020 (2020), https://doi.org/10.1155/2020/4912395.
[26] L.H. Wang, Q.G. Liang, Y. Zhang, F. Liu, Y. Sun, S.M. Wang, et al., iTRAQ-based quantitative proteomics and network pharmacology revealing hemostatic mechanism mediated by Zingiberis Rhizome Carbonisata in deficiency-cold and Hemorrhagic Syndrome rat models, Chem-Biol. Int. 343 (2021), https://doi.org/10.1016/j.cbi.2021.109465.
[27] J.B. Hou, W. Chen, H.T. Lu, H.X. Zhao, S.Y. Gao, W.R. Liu, et al., Exploring the therapeutic mechanism of Desmodium styracifolium on oxalate crystal-induced kidney injuries using comprehensive approaches based on proteomics and network pharmacology, Front. Phar. 9 (2021), https://doi.org/10.3389/fphar.2018.00620.
[28] J.D. Christopher, A. Wafaa, C. Andrew, S.H. Iain, T.G. Nikolaos, A clinical and biological guide for understanding chemotherapy-induced alopecia and its prevention, The Oncol 23 (1) (2018) 84–96, https://doi.org/10.1634/theoncologist.2017-0263.
[29] X. ang, H. Chen, R. Tian, et al., Macrophages induce AKT/β-catenin-dependent Lgr5+ stem cell activation and hair follicle regeneration through TNF, Nat. Commun. 8 (2017). https://doi-org.ezproxy.lib.szu.edu.cn/10.1038/ncomms14091.
[30] C.L. Ana, A.S. Robert, J.C. Philip, Facial bacterial infections: folliculitis, Clin. Dermatol. 32 (6) (2014) 11–714, https://doi.org/10.1016/j.clindermatol.2014.02.009.
[31] D.C. Saceda, C. Pindado, O.M. Moreno, et al., Association of inflammation with progression of hair loss in women with frontal fibrosing alopecia, JAMA Dermatol. 15696 (2020) 700–702, https://doi.org/10.1001/jamadermatol.2020.0359.
[32] Z. Guangpin, L. Changgui, Y. Xanyin, A Comparative study on estrogen receptors in human skin of various hairy regions, J. Clin. Dermat 2 (1994) 71–73..
[33] H. Huimin, Z. Shoubing, L. Xiaohua, D. Zhili, G. weixiang, Q. Zhifang, et al., Estrogen leads to reversible hair cycle retardation through inducing premature catagen and maintaining telogen, PLoS One 7 (7) (2012), https://doi.org/10.1371/journal.pone.0040124.
[34] F. Aimee, C. Sekyu, H. Ya-Chieh, E.L. William, Inhibition of pyruvate oxidation as a versatile stimulator of the hair cycle in models of alopecia, Experimental Dermat 30 (4) (2021) 448–456, https://doi.org/10.1111/exd.14307.
[35] S.W. Mitchell, A.G. Kurt, A. Sahar, S. Imran, J. David, et al., Validation of a genomics-based hypothetical adverse outcome pathway: 2,4-dinitrotoluene perturbs PPAR signaling thus impairing energy metabolism and exercise endurance, Toxi. Sci. 141 (1) (2014) 44–58, https://doi.org/10.1093/toxsci/kfu104.

[36] H. Lizhi, PPAR-Γ Agonists in the Preparation of Drugs for the Treatment of Alopecia Areata and Drugs for the Treatment of Alopecia Areata, 2017. CN106389457A[P].
[37] T. Rickmeyer, K. Jager, S. Schoniger, H.A. Schoon, Cytokeratin expression profiles of canine epithelial tissues, Histol. Histopathol. 34 (6) (2019) 683–696, https://doi.org/10.14670/HH-18-070.
[38] M.K. Heatley, Keratin expression in human tissues and neoplasms, Histopathol 41 (4) (2002) 365–366, https://doi.org/10.1046/j.1365-2559.2002.01387.x.
[39] R. Moll, M. Divo, L. Langbein, The human keratins: biology and pathology, Histochem. Cell Biol. 129 (6) (2008) 705–733, https://doi.org/10.1007/s00418-008-0435-6.
[40] B.K. Kim, I.C. Baek, H.Y. Lee, J.K. Kim, H.H. Song, S.K. Yoon, Gene expression profile of the skin in the 'hairpoor' (Hr(Hp)) mice by microarray analysis, BMC Genom. 11 (2010), https://doi.org/10.1186/1471-2164-11-640.
[41] M. van Steensel, M. Vreeburg, M.T. Urbina, P. López, F. Morice-Picard, M. van Geel, Novel and mutations associated with monilethrix, Exp. Dermatol. 24 (3) (2015) 22–24, https://doi.org/10.1111/exd.12624.
[42] M. Giesen, S. Gruedl, O. Holtkoetter, G. Fuhrmann, A. Koerner, D. Petersohn, Ageing processes influence keratin and KAP expression in human hair follicles, Exp. Dermatol. 20 (9) (2011) 759–761, https://doi.org/10.1111/j.1600-0625.2011.01301.x.
[43] S.E. Clements, T. Techanukul, J.E. Lai-Cheong, J.B. Mee, A.P. South, C. Pourreyron, et al., Mutations in AEC syndrome skin reveal a role for p63 in basement membrane adhesion, skin barrier integrity and hair follicle biology, Brit. J. Dermatol. 167 (1) (2012) 134–144, https://doi.org/10.1111/j.1365-2133.2012.10888.x.
[44] S.Y. An, H.S. Kim, S.Y. Kim, S.Y. Van, H.J. Kim, J.H. Lee, et al., Keratin-mediated hair growth and its underlying biological mechanism, Com, Biol. 5 (1) (2022), https://doi.org/10.1038/s42003-022-04232-9.
[45] J. Cai, L. Ma, Msx2 and Foxn1 regulate nail homeostasis, Gene 49 (6) (2011) 449–459, https://doi.org/10.1002/dvg.20744.
[46] S. Redler, S.M. Pasternack, S. Wolf, D. Stienen, J. Wenzel, M.M. Nothen, et al., A novel KRT86 mutation in a Turkish family with monilethrix, and identification of maternal mosaicism, Clin. Exp. Dermatol. 40 (7) (2015) 781–785, https://doi.org/10.1111/ced.12631.
[47] M. van Steensel, M. Vreeburg, M.T. Urbina, P. Lopez, F. Morice-Picard, M. van Geel, Novel KRT83 and KRT86 mutations associated with monilethrix, Exp. Dermatol. 24 (3) (2015) 222–224, https://doi.org/10.1111/exd.12624.
[48] T. Matsuda, T. Yamamoto, A. Muraguchi, F. Saatcioglu, Cross-talk between transforming growth factor-β and estrogen receptor signaling through Smad3, J. Biol. Chem. 76 (46) (2001) 42908–42914, https://doi.org/10.1074/jbc.M105316200.
[49] A. Hata, B.N. Davis, Control of microRNA biogenesis by TGF beta signaling pathway-A novel role of Smads in the nucleus, Cytokine, Growth F.R. 20 (5–6) (2009) 517–521, https://doi.org/10.1016/j.cytogfr.2009.10.004.
[50] N. Rong, P. Mistriotis, X.Y. Wang, G. Tseropoulos, N. Rajabian, Y.L. Zhang, et al., Restoring extracellular matrix synthesis in senescent stem cells, Faseb. J. 33 (10) (2019) 10954–10965, https://doi.org/10.1096/fj.201900377R.
[51] Y.X. Liang, X. Tang, X. Zhang, C.X. Cao, M. Yu, M.J. Wan, Adipose mesenchymal stromal cell-derived exosomes carrying MiR-122-5p antagonize the inhibitory effect of dihydrotestosterone on hair follicles by targeting the TGF-β1/SMAD3 signaling pathway, Int. J. Mol. Sci. 24 (6) (2023), https://doi.org/10.3390/ijms24065703.
[52] Y.Y. Ding, X.L. Xue, Z.F. Liu, Y. Ye, P. Xiao, Y.B. Pu, et al., Expression profiling and functional characterization of miR-26a and miR-130a in regulating zhongwei goat hair development via the TGF-β/SMAD pathway, Int. J. Mol. Sci. 21 (14) (2020), https://doi.org/10.3390/ijms21145076.
[53] Y.T. Li, W.X. Duan, L. Shen, X.L. Ma, J.X. Ma, Y. Zhang, et al., Shengji solution accelerates the wound angiogenesis of full-thickness skin defect in rats via activation of TGF-beta 1/Smad3-VEGF signaling pathway, Biot. Genet. (2023), https://doi.org/10.1080/02648725.2023.2196901.
[54] T. Yang, X. Zhang, A. Chen, Y. Xiao, S. Sun, J. Yan, et al., Progranulin promotes bleomycin-induced skin sclerosis by enhancing TGF-beta/Smad3 signaling through up-regulation of TGF-beta type I receptor, J. Invest. Dermatol. 139 (5) (2019) S8–S, https://doi.org/10.1016/j.ajpath.2019.04.012.
[55] E.Y. Caroline, A.O. Elise, Treatment of chemotherapy-induced alopecia, Dermat. Ther. 24 (4) (2011) 432–442, https://doi.org/10.1111/j.1529-8019.2011.01430.x.
[56] K. Donald, More than a, Journal. Sci. 291 (2001), https://doi.org/10.1126/science.291.5501.13, 13-13.
[57] J.J. Jimenez, A.A. Yunis, Protection from 1-β-d-arabinofuranosylcytosine-induced alopecia by epidermal growth factor and fibroblast growth factor in the rat model, Cancer Res. 52 (2) (1992) 413–415.
[58] D. Svein, S. Torril, L.J. Fridtjof, Epidermal growth factor receptor inhibition induces trichomegaly, Acta Oncol 42 (4) (2009) 345–346, https://doi.org/10.1080/02841860310006038.
[59] R.G. Belen, J. Margit, F. Jamie, A.M. Natasha, Pathogenesis and treatment options for chemotherapy-induced alopecia: a systematic review, Inter. Jour. Demart. 57 (12) (2018) 1417–1424, https://doi.org/10.1111/ijd.13906.